Systematic Optimization of an H_2 PEM Fuel Cell Power Generation System with Heat Integration

Cong Xu, Lorenz T. Biegler, and Myung S. Jhon
Dept. of Chemical Engineering, Carnegie Mellon University, Pittsburgh, PA 15213

DOI 10.1002/aic.10873
Published online April 20, 2006 in Wiley InterScience (www.interscience.wiley.com).

An H_2 Polymer Electrolyte Membrane (PEM) Fuel Cell power generation system composed of three subsystems: fuel reforming, fuel cell stack, and post combustion is examined. The system is simulated and optimized with a fuel cell model integrated within the process flow sheet. A case study optimization of the entire power generation system is presented and the influence of heat integration on the optimization is demonstrated. Our objectives are to maximize the energy and system efficiencies as well as the system profit. Here, optimization formulations with heat integration are used to realize our objectives, which explore the synergy between optimization and heat integration. Our results showed that we can achieve an energy efficiency as high as 58.30% and a system efficiency as high as 28.35%. For comparison, we provide results obtained from sequential process optimization followed by heat integration. The gain from the synergy is mostly exemplified in the profit maximization study, where the profit increases by almost 27.15% in the best case. Finally, we obtain optimization results that include feed vaporization of water to steam as a comparison for the heat integration. These results demonstrate the importance of simultaneous optimal heat integration for fuel cell-based processes. © 2006 American Institute of Chemical Engineers *AIChE J,* 52: 2496–2506, 2006
Keywords: fuel cell system, H_2 PEM fuel cell, heat integration, power generation, efficiency, cost optimization, fuel processing

Introduction

Over the last few years, fuel cells have attracted considerable attention as a potential replacement for current power generation and automobile engine systems. Fuel cells have the advantage of high power density, high efficiency, and zero or ultra-low emissions, and promise to ease concerns regarding fossil energy and the environment. Government and the industry supported research programs have concentrated on the development of operable fuel cells and their commercialization. In a "fuel cell report to Congress,"[1] cost and durability are the primary technical barriers to commercialization.

To reduce the cost and improve the durability of fuel cells, we need to understand the fuel cell at every level in order to provide the optimal process design. Since the modeling work should reflect the complexity of the overall process, unravel the interactions, and simplify input/output characteristics of components,[2] the National Energy Technology Laboratory (NETL) is currently developing a multi-level model of fuel cells, including micro or fundamental modeling, cell modeling, stack modeling, and system modeling. Many studies[3-8] describe the modeling of fuel cells. Starting from the early 90s, researchers[3,4,6,9] have developed simple 0-D models, some of which focused on separate parts in the fuel cells, such as the electrodes or the gas diffusion layers.[9] Recently, Springer et al.[5] developed a 1-D H_2 PEMFC model that examines the effect of CO poisoning and hydrogen dilution. Wang et al.[8] have modeled PEMFCs extensively and have extended the model to two and even three spatial dimensions.[7] Water and heat management have also been considered in their models since the temperature profiles can be easily obtained with higher dimensional models by incorporating computational fluid dynamics (CFD) techniques.

Correspondence concerning this article should be addressed to L. T. Biegler at lb01@andrew.cmu.edu.

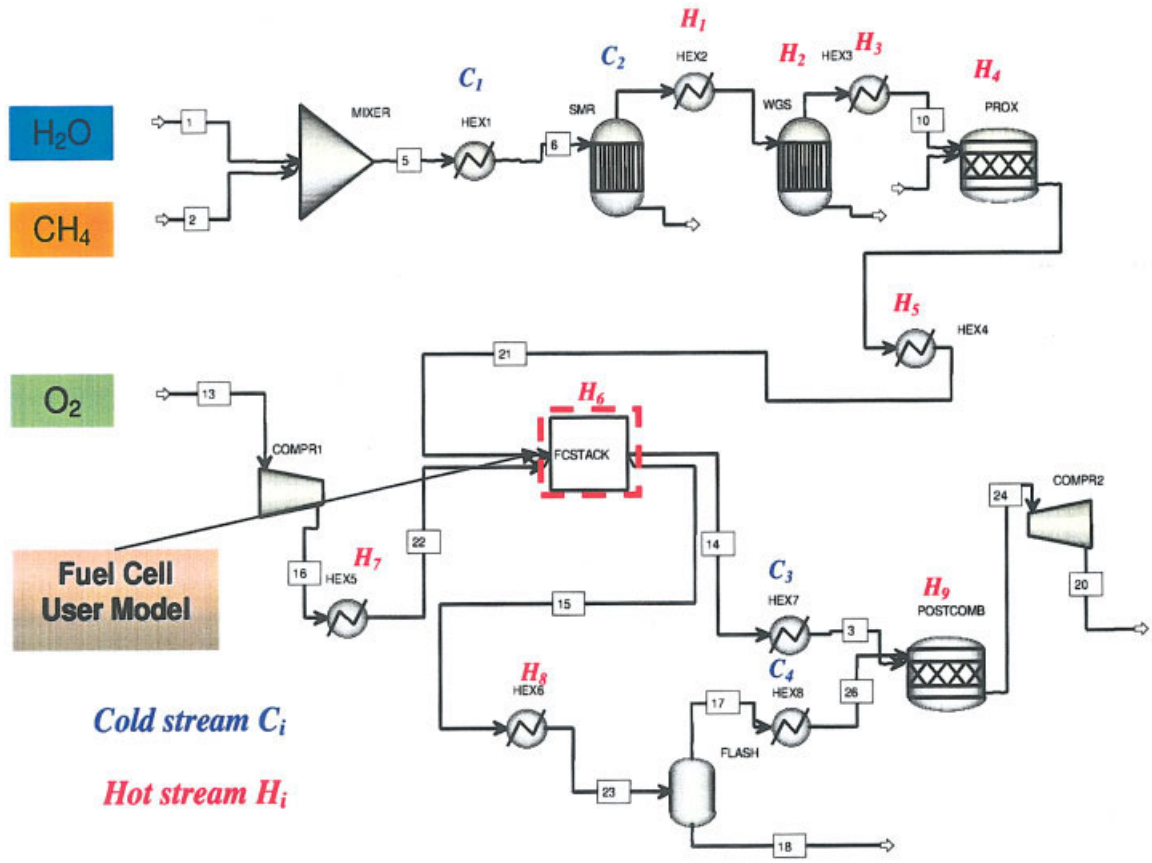

Figure 1. The ASPEN Plus flow sheet for the fuel cell system with hot and cold streams denoted.

[Color figure can be viewed in the online issue, which is available at www.interscience.wiley.com.]

Despite the rapid development of fuel cell modeling, there are few studies on fuel cell systems, including fuel reforming processes. To reduce the cost and improve the performance, it will be desirable to examine fuel cell behavior under the environment of the whole process. We not only need to understand cells and stacks, but also the supporting technology relevant to fuel cell development, such as fuel storage, fuel distribution, fuel reforming, post-combustion, and heat exchanger networks. Moreover, optimization has been in high demand for fuel cell design and operation. Since the late 90s, Moore and coworkers[10] have been working on the optimization of the overall energy conversion efficiency and concentrated on performance of DMFC stacks in automotive applications. They aimed to develop an operational strategy to achieve maximum efficiency by varying the methanol feed concentration and flow rate under a wide range of power demands. Similarly, we have recently performed an optimization study on a DMFC, which provides methanol feeding strategies both in the steady and dynamic states to achieve the maximum power output under various current densities.[11] Godat and Marechal[12] considered the effect of heat integration of the optimal performance of power generation systems that incorporate H_2 PEM fuel cells. They considered key variables of the fuel cell process and performed single variable optimizations along with sensitivity analysis of these heat integrated processes. More recently, Marechal and coworkers[13] extended this approach with a genetic algorithm for multi-objective optimization; they were able to consider structural flowsheet options as well as capital costs.

Our study also focuses on the optimization of this particular heat integrated PEM fuel cell power generation system. In addition to the work of Godat and Marechal,[12] it performs a systematic process optimization using an integrated heat integration formulation along with Sequential Quadratic Programming (SQP), a state-of-the-art nonlinear programming (NLP) algorithm. Using SQP within the Aspen Plus simulator, we consider the maximization of the fuel cell efficiency, as well as system efficiency and profit. Finally, heat exchanger network (HEN) structures are constructed to provide guidance for the optimal design and operation of the system.

In the following sections, we first introduce the fuel cell system for our simulation. We provide sensitivity studies for the flowsheet design variables and follow this with the description of simultaneous optimization strategy with heat integration. Then we provide our results about the minimization of the utility and system cost and the maximization of the system efficiency by manipulating key decision variables in the process flow sheet.

The Fuel Cell System

Our system model is based on work by Godat and Marechal[12] and builds on a flow sheet using the Aspen Plus[14] simulator, as shown in Figure 1. It consists of the hydrogen production process, fuel cell stacks, and a post combustion process. Typically, a steam reformer reactor running on natural

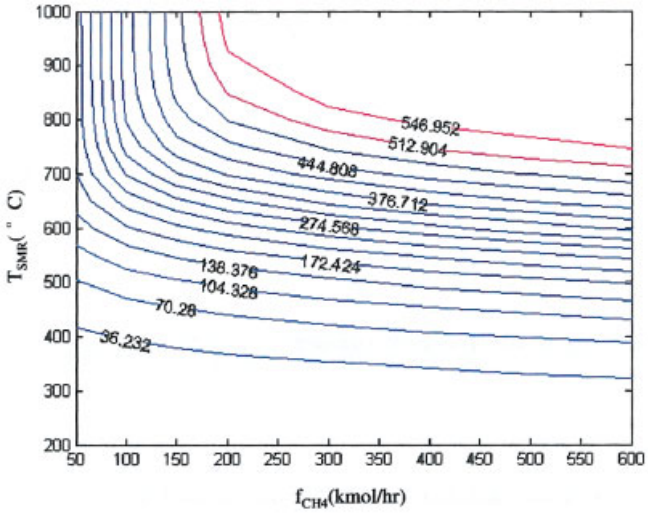

Figure 2. Anode H_2 inlet flow for different CH_4 feeding rates versus SMR reactor temperatures.

[Color figure can be viewed in the online issue, which is available at www.interscience.wiley.com.]

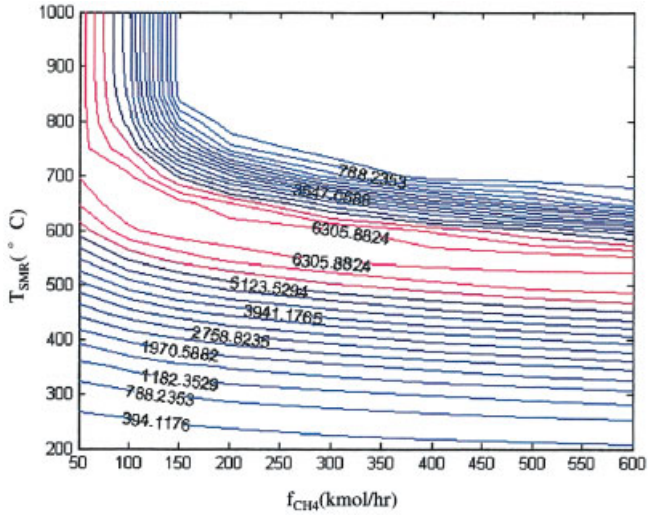

Figure 3. Case study on system power output under various CH_4 feeding rates and different T_{SMR}.

[Color figure can be viewed in the online issue, which is available at www.interscience.wiley.com.]

gas is chosen for the hydrogen generation. Since methane is the main component of natural gas, for simplicity we use pure methane as the inlet. Here, stream #1 is saturated steam feed at 3 bar and stream #2 is a pure methane feed provided at 3 bar and 25°C. The two streams are combined, heated to reactor temperature, and fed to the steam methane reforming (SMR) reactor, where methane and steam are reacted on a catalyst surface to produce hydrogen and carbon monoxide. Generally, the reformate from the steam reformer reactor is composed of 75% hydrogen and 10-15% carbon monoxide.[15]

For the PEM fuel cell application, the carbon monoxide content must be 10 ppm or less. To remove the carbon monoxide, the SMR reformate enters the water gas shift (WGS) reactor, where carbon monoxide reacts further with steam to produce hydrogen and carbon dioxide. Depending on the reformate composition, more than one shift reactor may be needed. In industrial practice, there might be a two-stage WGS system: a high (400-500°C) temperature WGS reactor followed by a low temperature (200-250°C) one. These two stages of shift conversion can reduce the content of carbon monoxide to a level as low as 2500 ppm. However, this is still not sufficient for the PEM fuel cell operation. A preferential oxidation (PROX) reactor is needed to further remove carbon monoxide. For simplicity, we only add one WGS reactor in the system, as in Godat and Marechal.[12] However, the PROX reactor will ensure the carbon monoxide content is decreased to the acceptable level, though some hydrogen may also be oxidized in the PROX reactor if the carbon monoxide inlet concentration is too high. In the flowsheet shown in Figure 1, the WGS effluent enters the PROX reactor along with a make-up system to oxidize the remaining CO in the stream. This stream consists of pure oxygen, required for the oxidation of CO. The effluent stream from the PROX reactor, which is hydrogen-rich with trace amounts of CO, is fed to the anode of the fuel cell stacks. A compressed oxygen stream (#13) is fed to the cathode of the fuel cell stacks. The outlet stream from the anode is a hydrogen-lean stream, while the cathode effluent contains both O_2 and H_2O. After removing H_2O in a flash separator, the O_2 stream combines with the anode effluent and enters the post-combustor where O_2 reacts with H_2. Finally, the hot outlet stream from the post combustor is depressurized and discharged to the atmosphere.

The SMR and WGS reactors are both modeled with approach to equilibrium reactor models (REquil) in ASPEN Plus. Reactions in the PROX and post-combustion (POSTCOMB) reactors essentially go to completion and are both modeled with the stoichiometric models (RStoic) in ASPEN Plus. All reactors are operated under isothermal conditions, and heat is supplied or removed to maintain the temperature in the reactor from an external hot or cold utility. In order to define appropriately the energy requirement of the heat exchange, we have assumed that the inlet streams are preheated up to the reaction temperature. To model them, we place heat exchangers before each unit to ensure that the inlet stream is at the same temper-

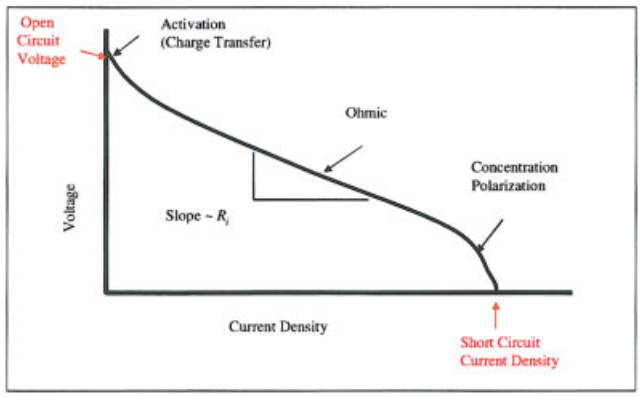

Figure 4. Generalized polarization curve for a fuel cell showing regions dominated by various types of losses.

[Color figure can be viewed in the online issue, which is available at www.interscience.wiley.com.]

Table 1. Energy Efficiency Optimization Results for Cases Where f_{CH4} Assumes Five Different Lower Bounds, Respectively

LB (kmol/hr)	f_{CH_4}* (kmol/hr)	T_{SMR}* (°C)	T_{WGS}* (°C)	P_{cell} (kW)	Efficiency
50.00	50.00	780.00	236.44	6505.76	58.30%
80.00	80.00	679.00	244.81	6714.02	37.60%
100.00	100.00	655.48	245.85	6701.60	30.03%
120.00	120.00	647.87	250.84	6673.95	24.92%
150.00	150.00	627.52	252.27	6664.47	19.91%

*Denotes optimal values.

ature. Like the construction of pinch curves, the process integration optimization formulation allows us to avoid detailed construction of the complex heat exchange network within the heat integrated system.

The fuel cell system is composed of three subsystems as follows:

(1) The fuel processing (FP) subsystem.
(2) The PEMFC stack subsystem.
(3) The post-combustion subsystem.

Fuel reforming

The fuel processing subsystem includes the following three main reactors:

(1) To produce hydrogen from methane, the SMR proceeds with two reactions: endothermic reforming of methane and steam, $CH_4 + H_2O <==> 3H_2 + CO$, and an exothermic water gas shift (WGS) reaction, $CO + H_2O <==> CO_2 + H_2$.

(2) By reacting CO with steam, the WGS reactor produces additional hydrogen through the water gas shift reaction, but at an operating temperature lower than the SMR reactor.

(3) The PROX reactor converts the remaining CO into CO_2, by the reaction $CO + ½\ O_2 <==> CO_2$, to avoid poisoning the fuel cell membrane. However, the catalyst is nonselective and some hydrogen in the gas stream is also combusted according to $H_2 + ½\ O_2 <==> H_2O$.

Further details of the SMR, WGS, and PROX reactors can be found in Godat and Marechal.[12]

Fuel cell stack model

The fuel cell stack model is equilibrium based and adopted from Godat and Marechal.[12] The model equations are given as follows:

$$U_{Nernst} = U^0_{Nernst}(T_{cell}) + \frac{RT_{cell}}{2F}\ln\left(Y^{H_2}_{anode}(Y^{O_2}_{anode})^{1/2}\Big/ Y^{H_2O}_{anode}\right) + \frac{RT_{cell}}{4F}\ln(p_{cell})$$

$$V_{cell} = U_{Nernst} - R_{cell}i_{cell}$$

$$i_{cell} = I_{cell}/A_{cell}$$
$$I_{cell} = 2Fn^{H_2}_{i,cathode}$$
$$P_{cell} = V_{cell}I_{cell} \quad (1)$$

Here, U_{Nernst} is the cell voltage adjusted to the cell temperature (T_{cell}), pressure (p_{cell}), and component mole fractions (Y^{ξ}) of species ξ, V_{cell} is the cell voltage, i_{cell} is the current density, I_{cell} is the current, P_{cell} is the power output of the cell, R_{cell} is the internal resistance of the cell, and A_{cell} is the cross sectional area of the cell, respectively. From Eq. 1, we find that T_{cell} and p_{cell} have a significant effect on the value of V_{cell}. These decision variables should be set at their upper bounds and practical limits from other studies. The modern PEM fuel cells operate at a 60-100°C range.[15] Generally, the higher the temperature, the better the performance will be, mainly due to cathode overpotential reduction. Since 100°C is the water vaporization point, close to 100°C cell temperature will raise significant difficulty to maintain a reasonable humidity level inside the PEM. However, Larminie and Dicks[15] show it is viable to run the fuel cell at temperatures as high as 90°C without causing the PEM to dry out. So we set T_{cell} and p_{cell} to be 90°C and 3 bar, respectively. Since we operate all the other components of the system under constant pressure, it is also valid to operate the stacks this way.

Post combustion

The post combustion subsystem burns the depleted fuel of the PEMFC subsystem and generates heat that is used to balance the energy requirement of the fuel processing section. Complete combustion is assumed using a stoichiometric model. The stream at the cathode outlet is cooled down and the water is separated and possibly recycled into the steam methane reformer.

Heat Integration

The idea of simultaneous optimization and heat integration of chemical processes was initially proposed by Duran and Grossmann.[16] Lang et al.[17] and Yee et al.[18] improved this approach and expanded its application for flowsheet simulators and MINLP process design, respectively. Note that the heat exchange network is not considered directly in the simulation model described above. Instead, an optimization formulation related to pinch technology can be used to model the integrated heat exchange system without having to impose a heat exchange network structure. A typical heat integration optimization problem using pinch technology can be described as follows:

$$\min C = \phi(x) + c_sQ_s + c_wQ_w$$

Table 2. System Efficiency Optimization Results With and Without Heat Integration (HI) for LB = 50

Cases	f_{CH_4}* (kmol/hr)	T_{SMR}* (°C)	T_{WGS}* (°C)	P_{cell} (kW)	Qs (kW)	Qw (kW)	Efficiency
Simultaneous optimization with HI	50.00	780.00	278.00	6497.10	4922.02	6854.21	28.35%
Sequential optimization with HI	50.00	780.00	234.39	6506.18	5030.79	6964.43	28.10%
Optimization without HI	50.00	780.00	234.39	6506.18	10418.95	8852.44	21.38%

Table 3. Cost Coefficients[22] Values for the System

Cost Coeff.	C_S ($/kWh)	Cw ($/kWh)	Cp ($/kWh)	C_{CH4} ($/kmol)
Value	0.0147	0.0017	0.0921	2.8739

C_s is for the hot utility, that is, natural gas; C_w is for the cold water utility; C_p is for the power output; C_{CH4} is for the CH_4 inlet stream.

s.t.

$$h(x) = 0$$
$$g(x) \le 0$$
$$Q_s \ge \sum_{j=1}^{n_c} f_j[\max\{0,\ t_j^{out} - (T^p - \Delta T_{\min})\} - \max\{0,\ t_j^{in} - (T^p - \Delta T_{\min})\}] - \sum_{i=1}^{n_H} F_i[\max\{0,\ T_i^{in} - T^p\} - \max\{0,\ T_i^{out} - T^p\}], \quad p \in \Pi$$
$$Q_w = Q_s + \Omega$$
$$\Omega = \sum_{i=1}^{n_H} F_i(T_i^{in} - T_i^{out}) - \sum_{j=1}^{n_C} f_i(t_j^{out} - t_j^{in}) \qquad (2)$$

where $\phi(x)$ is the cost/profit function other than utility cost, Ω is the heat surplus of the system, Q_s is the requirement of the hot utility, Q_w is the requirement of the cold utility, $h(x)$ is the ASPEN Plus flow sheet model, $g(x)$ represents the inequality constraints, j is the index for cold streams in the flow sheet, i is the index for hot streams, t_j is the temperature of cold stream j, T_i is the temperature of hot stream i, and F_i and f_j are the heat capacity flowrates for the hot and cold streams, respectively. The index set Π defines candidate pinch points from inlet temperatures of hot and cold streams; T_p, $p\varepsilon\Pi$ is the candidate pinch temperature defined as follows:

$$T_P = \begin{cases} T_i^{in} \text{ if candidate } p \text{ is hot stream } i \\ t_j^{in} + \Delta T_{\min} \text{ if candidate } p \text{ is cold stream } j \end{cases} \qquad (3)$$

$\Delta T_{\min}$ is the minimal temperature interval that is possible for the heat exchange to take place, which is set to be 20°C in our study. The number of pinch temperature candidates is determined by the total number of hot and cold streams. The right hand side of the inequality for Q_s in Eq. 2 represents the difference between the heat contents of the cold and hot streams (heat deficit) above any candidate pinch $p\varepsilon\Pi$. The problem is then posed to find the smallest value of Q_s such that all the inequalities hold; Q_s, therefore, equals the maximal value of the heat deficit. The temperature T^p where the heat deficit achieves this maximum is the pinch point.

Note that the above formulation can treat the flows and the temperatures as variables for the optimization and the heat integration. The remaining difficulty is the presence of nondifferentiable max operators in Eq. 2. As shown in Eq. 4, a smoothing approximation procedure can be used that avoids difficulties with the use of NLP solvers.[19,20]

$$\max\{0, f(x)\} = 0.5[f(x)^2 + \varepsilon^2]^{1/2} + 0.5f(x) \qquad (4)$$

where ε usually assumes a relatively small value (such as 10^{-3} in our study).

The optimization formulation (Eq. 2) is applied to a number of fuel-cell optimization cases in the next section. Each of these optimization problems was solved with the SQP solver in Aspen Plus. Because SQP is an efficient gradient-based NLP solver, optimizations of all of these cases were obtained quite efficiently, within an order of magnitude of the effort required for a single flowsheet simulation.

Results and Discussion

Sensitivity analysis on H_2 inlet versus CH_4 inlet and T_{SMR}

There are many variables in the system that can be chosen as the decision variables for an optimization problem. We ran the case study to choose the most sensitive ones, such as T_{SMR}, T_{WGS}, T_{comb}, f_{CH4}, and f_{H2O}, using the sensitivity analysis in ASPEN Plus's model analysis tool. Here, f_ξ denotes the feed flow rate of species ξ.

The H_2O and CH_4 inlet streams have a similar effect on the conversion of H_2; either of them can be fixed relative to the other. For convenience, we set the H_2O inlet flow rate at a constant value (200 kmol/hr) and choose f_{CH4} as the decision variable.

Generally, if we increase the inlet flow rate of the H_2O and CH_4 or T_{SMR}, more H_2 is produced. When T_{SMR} is at 200°C or below, almost no H_2 is produced because the catalyst for the SMR reaction is inactive at this relatively low temperature. Similarly, we noticed that after T_{SMR} reached 800°C, further increase of T_{SMR} does not have a significant positive effect on the production of the H_2; this is thermodynamically consistent with the result in Lutz et al.[21] Also, Figure 2 provides a rough estimate on the lower and upper bounds that could be set for the decision variables. For example, H_2 production is much more sensitive to CH_4 inlet flow rate in the range between 50 and 200 kmol/hr than outside of this range.

The WGS temperature shows far less sensitivity to H_2 production, although we include it in the optimization studies below. Finally, we observe that the high post-combustor temperature T_{comb} has no influence on hydrogen conversion.

Table 4. Simultaneous System Profit Optimization Results with Heat Integration

LB (kmol/hr)	f_{CH_4}* (kmol/hr)	T^*_{SMR} (°C)	T_{WGS}* (°C)	P_{cell} (kW)	Energy Efficiency	Qs (kW)	Qw (kW)	Profit ($/hr)
50.00	50.00	780.00	257.60	6502.00	58.27%	4922.00	6855.00	370.70
100.00	100.00	650.81	256.29	6697.00	30.01%	5551.46	8535.82	232.79
150.00	150.00	618.69	245.57	6667.00	19.91%	6036.52	8488.49	79.31

Table 5. System Profit Optimization Results Without Heat Integration

LB (kmol/hr)	f_{CH_4}* (kmol/hr)	T_{SMR}* (°C)	T_{WGS}* (°C)	Qgen (kW)	Qsink (kW)	Total$Q$ (kW)	Profit_NoHI ($/hr)
50.00	50.00	780.00	257.60	10420.00	8488.00	18908.00	286.90
100.00	100.00	650.81	256.29	12274.00	9290.00	21564.00	132.47
150.00	150.00	618.69	245.57	12535.00	10084.00	22619.00	−19.21

Cell performance

Cell power output is a key measure of the performance of the power generation system. The cell power equals to the product of cell voltage and current:

$$P_{cell} \equiv V_{cell} I_{cell} \tag{5}$$

Figure 3 shows how the two decision variables would affect the performance of the system. We already know that high T_{SMR} or f_{CH4} are generally beneficial for H_2 production.

On the other hand, the current of the fuel cell stack is correlated with the anode H_2 inlet by the following equation:

$$I_{cell} = 2 \cdot F \cdot f_{H_2}^{reacted} \tag{6}$$

Here, F is the Faraday constant and $f_{H_2}^{reacted}$ is the amount of H_2 reacted to produce power in the stack. We assume a constant conversion ratio for the H_2 such that $f_{H_2}^{reacted}$ is directly proportional to the H_2 inlet flow rate. The conversion ratio is also known as the fuel utilization parameter, which we assume to be 95% as was commonly used in the literature.[12] The characterization curve of the fuel cell stack is the polarization curve (Figure 4).

Typically, if current is zero, cell voltage is at its maximum value, called OCV (open circuit voltage). As current increases, the cell voltage decreases due to various polarizations inside the cells. After current reaches a limit current, the cell voltage becomes zero. This explains the zero power densities in the upper right hand corner of Figure 3. This phenomenon also confirms that there exist optimal values for the T_{SMR} under different CH_4 inlet conditions to maximize the power output. For example, when T_{SMR} equals about 600°C, increasing the CH_4 inlet flow rate from 200 kmol/hr leads to decreasing power output.

Efficiency analysis

The above case studies provide us with an understanding of the effect of the two decision variables in the following optimization problem formulation. We first focus on the efficiency. There are two efficiencies to evaluate the system; one is the energy efficiency and the other is the system efficiency. The energy efficiency only considers the conversion rate of the fuel source energy to the cell power, which can be defined as follows:

$$\eta_{energy} \equiv \frac{P_{cell}}{P_{combustion}} \equiv \frac{V_{cell} \cdot i_{cell}}{f_{CH_4} \cdot LHV_{CH_4}} \tag{7}$$

where LHV_{CH4} denotes the lower heating value of methane.

The system efficiency can be defined as:

$$\eta_{sys} \equiv \frac{V_{cell} \cdot i_{cell}}{f_{CH_4} \cdot LHV_{CH_4} + Q} \tag{8}$$

where Q is the additional energy consumed to operate the system. This quantity consists mostly of the hot and cold utilities.

Optimal energy efficiency

The optimization problem can be defined as follows:

$$\begin{aligned} \max_{\{f_{CH_4}^{in}, T_{SMR}\}} \quad & \eta_{FCsys} = \frac{P_{cell}(f_{CH_4}, T_{SMR}, y)}{LHV_{CH_4} \cdot f_{CH_4}} \\ s.t. \quad & h(f_{CH_4}, T_{SMR}, T_{WGS}, y) = 0 \\ & LB \le f_{CH_4} \le 200 \text{ kmol/h} \\ & 420 \le T_{SMR} \le 780°C \\ & 200 \le T_{WGS} \le 400°C \end{aligned} \tag{9}$$

where the equation $h(f_{CH4}, T_{SMR}, T_{WGS}, y) = 0$ represents the ASPEN Plus flow sheet model. The lower and upper bounds for f_{CH4} and T_{SMR} were chosen according to the results obtained from the sensitivity analysis. The range of T_{SMR} is determined from the thermodynamic analysis of the hydrogen production by steam reforming.[22]

As is shown in Table 1, optimal energy efficiency can be as high as 58.3% in our study when f_{CH4} assumes the lower bound value of 50 kmol/hr and T_{SMR} is at the upper bound, 780°C. As the CH_4 inlet rate increases, the energy efficiency decreases sharply before it reaches 100 kmol/hr and levels off afterwards. The optimal T_{SMR} also decreases accordingly until it reaches a lowest value at 627°C.

System efficiency

By considering the heat and cold utility consumption in the whole system, we get the overall efficiency of the power generation system. This can be denoted as the cell power over

Table 6. Comparison of the System Profit Optimization Results Between Cases With and Without Heat Integration

LB (kmol/hr)	Profit_NoHI ($/hr)	Profit_HI ($/hr)	Percentage Gain with HI
50.00	286.90	370.70	29.21%
100.00	132.47	232.79	75.73%
150.00	−19.21	79.31	N/A

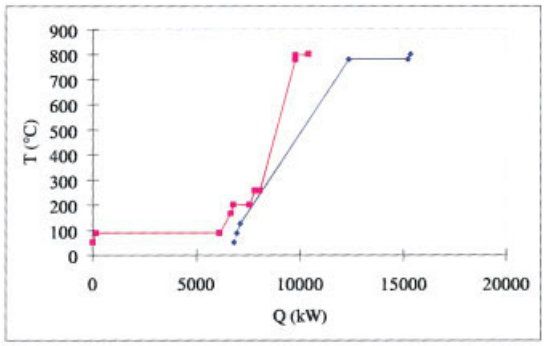

(a)

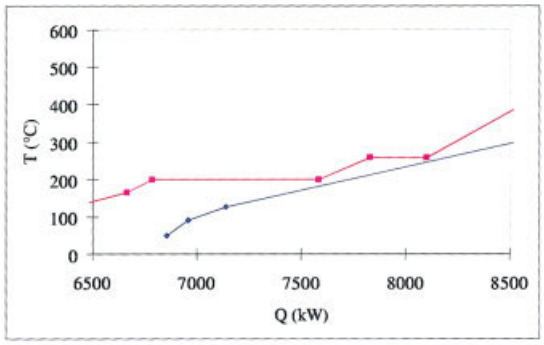

(b)

Figure 5. Comparison of the profit for cases with and without heat integration.

[Color figure can be viewed in the online issue, which is available at www.interscience.wiley.com.]

the total of the fuel and utility energy consumption. Similar to the energy efficiency case, we can formulate the system efficiency optimization problem as follows:

$$\begin{aligned} \max_{\{f_{CH_4}^{in},\, T_{SMR}\}} \quad & \eta_{FCsys} = \frac{P_{cell}(f_{CH_4}, T_{SMR}, y)}{LHV_{CH_4} \cdot f_{CH_4} + Q_s + Q_w} \\ s.t. \quad & h(f_{CH_4}, T_{SMR}, y) = 0 \\ & LB \le f_{CH_4} \le 200 \\ & 420 \le T_{SMR} \le 780 \\ & 200 \le T_{WGS} \le 400 \end{aligned} \tag{10}$$

Here Q_s and Q_w result from the heat integration calculation. Compared to energy efficiency, the optimal value of the system efficiency is correspondingly lower due to the consideration of the utility consumption, which is comparable to the power generated, as is shown in Table 2. The maximal system efficiency is about 28.35%. The corresponding CH_4 inlet flow rate, T_{SMR}, and T_{WGS} are 50 kmol/hr, 780°C and 278°C, respectively. The lower bound can be explained because the f_{CH4} term appears in the denominator of the efficiency, which has a dominant effect on the objective value. T_{SMR} is at the upper bound because the SMR reaction is decisive to convert CH_4 to H_2. Since the SMR reaction is endothermic, higher reaction temperature benefits the conversion rate a lot. Also from Table 2, we observe a big difference between the utility requirements of the system with and without heat integration. The utility decreases by 38% with heat integration. We see that heat integration improves the system efficiency by about 6.7%, which is a significant achievement from the simultaneous optimization with heat integration.

Sequential optimization and heat integration

To show the importance of simultaneous optimization with heat integration, we carry out a sequential optimization study. We first perform the process optimization without heat integration, then followed by heat integration. The optimization problem formulation is largely the same as in Eq. 10 except that Q_s and Q_w are simply the hot and cold utility requirements of the system. As expected, we obtain different optimal values for certain decision variables than those from simultaneous optimization: methane flow rate and temperature of SMR are the same while temperature of WGS is different. Next, we perform heat integration based on the settings from the process optimization and obtain the system efficiency. From Table 2, we can see that the optimal efficiency results from simultaneous optimization are approximately 0.25% higher than the sequential optimization results.

Profit optimization

The total system profit equals the revenue from the power generated by the fuel cell stack minus utility cost and the cost of the material (methane only). For cost coefficients, refer to Table 3. The corresponding minimization problem can be represented as follows:

$$\min C = c_s Q_s + c_w Q_w - c_p P_{cell} + c_{CH_4} f_{CH_4}$$

s.t.

$$\begin{aligned} h(x) &= 0 \\ g(x) &\le 0 \end{aligned}$$

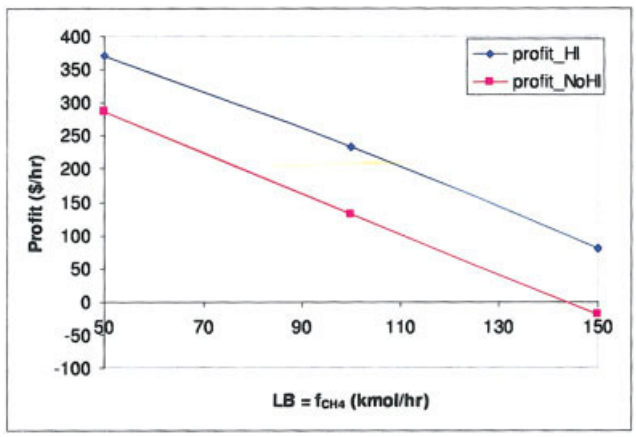

Figure 6. The composite curves of the system with a steam to carbon ratio of 4:1 and T_{SMR} of 780°C, and T_{WGS} of 258°C.

(b) is an expansion of (a) near the pinch points. [Color figure can be viewed in the online issue, which is available at www.interscience.wiley.com.]

Table 7. Comparison of the System Profit Optimization Results Between Sequential Optimization (SequOpt) and Simultaneous Optimization (SimulOpt)

LB (kmol/hr)	f_{Ch_4}* (kmol/hr)	T_{SMR}* (°C)	T_{WGS}* (°C)	Profit_SequOpt ($/hr)	Profit_SimulOpt ($/hr)	$ Gain With SimulOpt
50.00	50.00	713.00	200.00	358.79	370.70	3.32%
100.00	100.00	615.25	200.00	212.08	232.79	9.77%
150.00	150.00	589.83	200.00	62.37	79.31	27.15%

$$Q_s \geq \sum_{j=1}^{n_c} f_j[\max\{0,\ t_j^{out} - (T^p - \Delta T_{\min})\} - \max\{0,\ t_j^{in} - (T^P - \Delta T_{\min})\}] - \sum_{i=1}^{n_H} F_i[\max\{0,\ T_i^{in} - T^p\} - \max\{0,\ T_i^{out} - T^p\}]$$

$$Q_w = Q_s + \Omega$$

$$\Omega = \sum_{i=1}^{n_H} F_i(T_i^{in} - T_i^{out}) - \sum_{j=1}^{n_C} f_j(t_j^{out} - t_j^{in})$$

$$LB \leq f_{CH_4} \leq 200$$
$$420 \leq T_{SMR} \leq 780$$
$$200 \leq T_{WGS} \leq 400 \qquad (11)$$

We initially set the lower bound of f_{CH4} to be 50.0 kmol/h. The optimal f_{CH4} hits the lower bound. Then we raise the lower bound in the following two cases, that is, 100.0 and 150.0 kmol/h, respectively. As seen in Table 4, the optimal f_{CH4} hits the lower bound in both cases. The methane cost occupies approximately 25% of the revenue when f_{CH4} is around 50.0 kmol/h; as we increase the lower bound of f_{CH4}, the cost percentage for methane increases tremendously. This contributes to the reason why the optimal value of f_{CH4} hit the lower bound. And we observe a sharp decrease in the profit. For the case that f_{CH4} assumes the lower bound of 150 kmol/h, the system loses its profitability without heat integration; with heat integration it is still profitable. From these results, we can conclude that a steam to carbon ratio of 4:1 is the optimal operating condition for this system, since we not only achieve the largest profit, but almost the highest energy efficiency (58% in this case). For comparison purposes, the system profit without heat integration was listed in Table 5. In Table 6 we made a brief comparison between the results with and without heat integration. With heat integration, we can increase the profit by at least 29%. The corresponding curves are shown in Figure 5. We observe a significant decrease in profit since utility cost occupies a big portion of the total cost. This is the key contribution from heat integration.

As with system efficiency, we also performed a sequential optimization study of the system profit problem. The results are shown in Table 7. The optimal values for temperature of WGS all hit the lower bounds, and the optimal SMR temperatures are correspondingly lower than the results from simultaneous optimization. Simultaneous optimization improves the sequential optimization results in a range from 3.32% to 27.15%. This

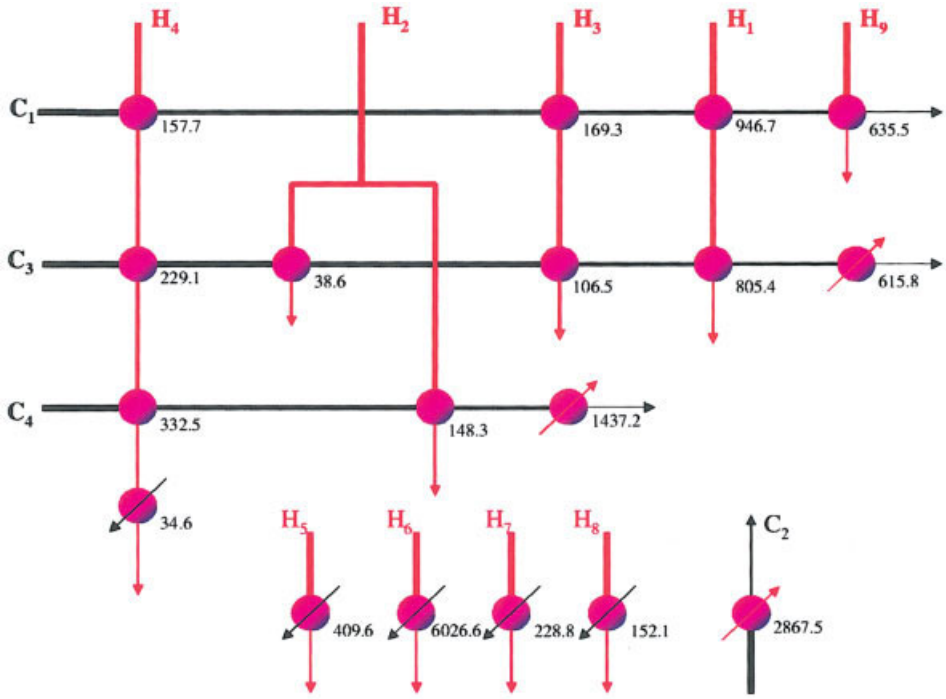

Figure 7. The suggested HEN for the system with a steam to carbon ratio of 4:1 and T_{SMR} of 627°C, and T_{WGS} of 258°C.

Heat duties (kW) are given for each exchanger. [Color figure can be viewed in the online issue, which is available at www.interscience.wiley.com.]

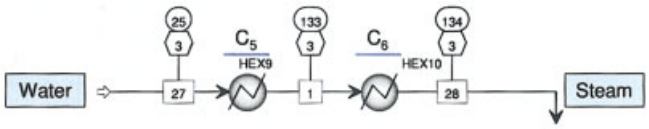

Figure 8. Part of the flowsheet that converts water feed (25°C) to steam (134°C) at pressure of 3 bar.

[Color figure can be viewed in the online issue, which is available at www.interscience.wiley.com.]

again shows the significance in carrying out the simultaneous optimization study.

The composite curves for the optimal operational conditions for f_{CH4} at 50 kmol/h are shown in Figure 6. Here, we can see that the heat exchange network utilizes most of the heat, except for the heat generated by the fuel cell stacks to cover the heat sink from the cold streams, other than the SMR reactor. External cold utility should be provided mainly for fuel cell stacks. Similarly, external hot utility should be used for the SMR reactor. If we expand the curves near the pinch point, then we can clearly see more detailed heat integration behavior. Here, the temperature of the WGS (258°C) and the PROX (200°C) are the two pinch points, which are the bottlenecks in developing the HEN. The corresponding HEN is shown in Figure 7.

Case Study with Water Instead of Steam as Process Feed

Up to this point, we chose steam as the process feed. Considering the fact that water at 25°C might also be used as the feed, we provide our study results with water feed as a comparison. In this case, as is shown in Figure 8, we first raise the temperature of the water from 25°C to 133°C, which is very close to the boiling point (133.5°C) at 3 bar using heat exchanger HEX9. Then, we realize the state conversion of water to steam via HEX10. Hence, according to our previous definition, we add two cold streams (C5 and C6) to the whole flowsheet that requires heat. That is the only difference between this flowsheet and the previous one. Since the change in the cold streams would affect the results of heat integration, we expect that the results for the optimal system efficiency and profit would change accordingly, as shown below.

Optimal System Efficiency with Water Feed

The problem statement is the same as Eq. 10. We provide our optimization results in Table 8. Compared to steam feed, the optimal system efficiency is slightly lower for cases with and without heat integration. The optimal SMR reactor temperature still hits the upper bound. However, the optimal WGS reactor temperature is 233°C instead of 278°C in the steam feed case.

To see the details of the heat integration, we draw the

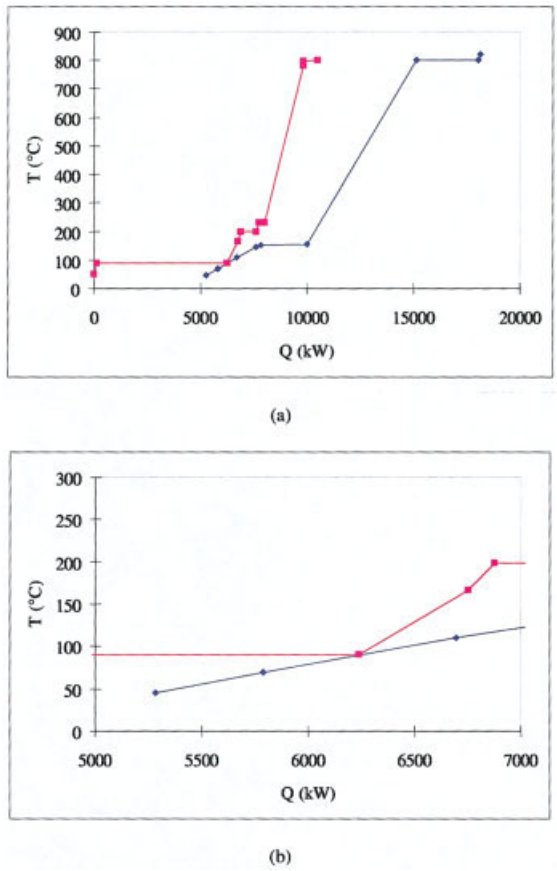

Figure 9. The composite curves of the system with a steam to carbon ratio of 4:1, T_{SMR} of 780°C, and T_{WGS} of 233°C.

(b) is an expansion of (a) near the pinch points. [Color figure can be viewed in the online issue, which is available at www.interscience.wiley.com.]

composite curves in Figure 9. We can see the effect of the water feed on the heat integration clearly from the composite curves. The pinch point is now 90°C. And we can now utilize the heat generated from the fuel cell to cover part of the heat requirement for converting the water liquid to steam. Due to the additional two cold streams in the water feed case, the total heat requirement increases significantly. We can see the optimal efficiency decreases by 2.72 percent (from 21.61% in the steam feed case to 18.89%) without heat integration. However, with heat integration, the optimal efficiency only decreases by 1.38 percent (from 28.35% to 26.97%), which is around half of the decrease in the case without heat integration. This reflects the importance of heat integration in adjusting to the change of operating conditions by trying to maintain the most efficient way to operate the system.

The HEN is shown in Figure 10. The hot and cold steams are

Table 8. System Efficiency Optimization Results With Water Feed for Cases With and Without Heat Integration (HI) With LB = 50

Cases	f_{CH_4}* (kmol/hr)	T_{SMR}* (°C)	T_{WGS}* (°C)	Pcell (kW)	Qs (kW)	Qw (kW)	Efficiency
With HI	50	780	232.56	6513.74	7664.49	5284.58	26.97%
Without HI	50	780	232.56	6513.74	10469	12849	18.89%

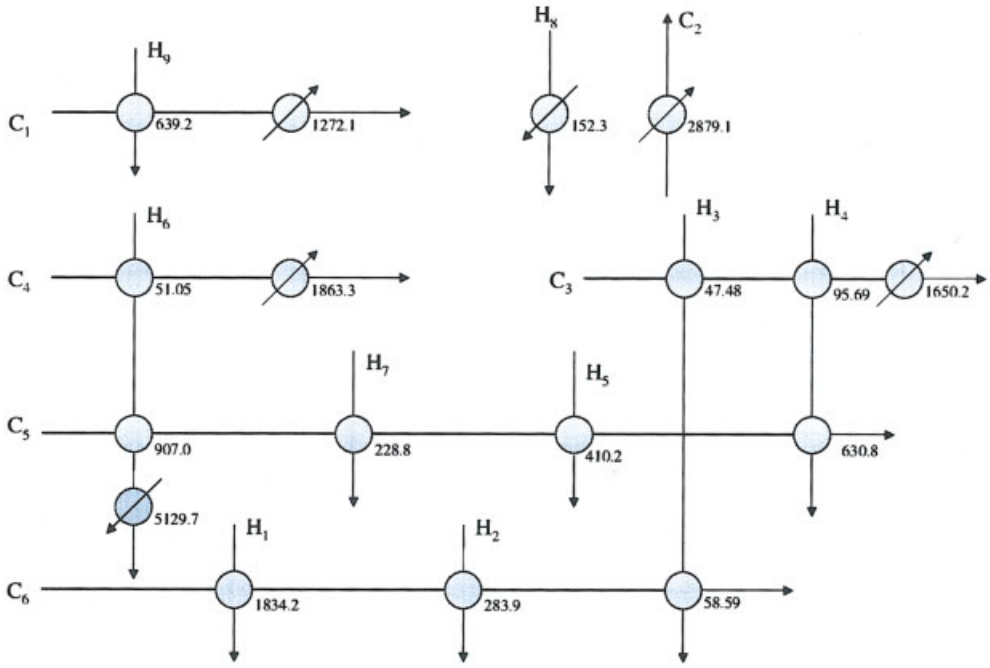

Figure 10. The suggested HEN for the system with a steam to carbon ratio of 4:1, T_{SMR} of 780°C, and T_{WGS} of 233°C.

Heat duties (kW) are given for each exchanger. [Color figure can be viewed in the online issue, which is available at www.interscience.wiley.com.]

"more" integrated in the sense that only hot stream H_8 is totally dependent on the external cold utility while the rest of the hot streams either totally or partially utilized the internal cold streams. This also explains why the optimal efficiency of the system doesn't decrease much with two additional cold streams in the water feed case.

Optimal System Profit with Water Feed

The problem statement is the same as Eq. 12. The optimal solution is provided in Table 9. Optimization without heat integration and a comparison are in Tables 10 and 11, respectively. Compared to the steam feed case, the optimal system profit is correspondingly lower. Both the composite curves in Figure 9 and HEN in Figure 10 still apply here in the case with 50.00 methane flow rate. In the cases with 100.00 and 150.00 as the lower bound for the methane inlet, the optimal WGS reactor temperature hits the upper bound (400°C).

Conclusions

We perform the simulation and optimization of a typical power generation system using ASPEN Plus. The CH_4 inlet flow rate, the WGS reactor temperature, and the temperature of the SMR reactor are the main decision variables in our study. The optimization is concentrated on efficiency improvement and profit maximization, which are goals of the current fuel cell development. We also perform a sensitivity case study on the fuel cell performance characterized by the power output. Since the water feed and steam feed are both considered in industrial systems, we provide results for both of them as a comparison. From the results, we can see the importance of simultaneous

Table 9. System Profit Optimization Results With Heat Integration in the Water Feed Case

LB $= f^*_{CH_4}$ (kmol/hr)	T^*_{smr} (°C)	T^*_{wgs} (°C)	P_{cell} (kW)	Energy Efficiency	Qs (kW)	Qw (kW)	Profit ($/hr)
50.00	780.00	232.56	6513.74	58.37%	7664.49	5284.58	333.52
100.00	667.24	400.00	6699.99	30.02%	7508.09	7336.77	206.31
150.00	632.61	400.00	6667.78	19.92%	8069.99	7401.37	51.25

Results are listed for cases where the lower bound for f_{CH4} was set to be 50.00, 100.00, and 150.00, respectively.

Table 10. System Profit Optimization Results Without Heat Integration in the Water Feed Case

$LB = f^*_{CH_4}$ (kmol/hr)	T^*_{SMR} (°C)	T_{WGS}* (°C)	Qgen (kW)	Qsink (kW)	Total$Q$ (kW)	Profit_NoHI
50.00	780.00	232.56	10469.00	12849.00	23318.00	279.75
100.00	667.24	400.00	13793.69	13965.00	27758.69	102.31
150.00	632.61	400.00	14099.69	14768.00	28867.69	−50.25

Table 11. Comparison of the System Profit Optimization Results Between Cases With and Without Heat Integration for Water Feed

LB = f_{CH_4} (kmol/hr)	T^*_{SMR} (°C)	T_{WGS}* (°C)	Profit_NoHI ($/hr)	Profit ($/hr)	Percentage Gain With HI
50	780.00	232.56	279.75	333.52	19.22%
100	667.24	400	102.31	206.31	101.66%
150	632.6141	400	−50.25	51.25	N/A

optimization with heat integration in balancing the heat requirement of the system and adjusting to the change of the operational conditions. The significance of simultaneous optimization is illustrated by comparing with the results from sequential optimization in system efficiency and profit optimization with steam feed.

As future work, we will generalize our model to include more detailed fuel cell and reactor models. Also, the capital costs of the process flowsheet and heat integration network were not considered, which might influence our simulation and optimization results. In a more complete study, a mixed integer nonlinear programming (MINLP) formulation will be very helpful to determine the selection of process equipment, the HEN, and the utility system.

Acknowledgments

PITA (Pennsylvania Infrastructure and Technology Alliance) administered by the Institute of Complex Engineered Systems (ICES) at Carnegie Mellon University is gratefully acknowledged for the financial support of this project.

Literature Cited

1. Garman DK. *Fuel Cell Report to the Congress* (Esecs Ee-1973), 2003.
2. Gemmen RS, Selman JR. Speeding the progress of fuel cell development. Proceedings of the NETL Workshop on Fuel Cell Modeling, Morgantown, WV, 2000.
3. Fuller TF, Newman J. Water and thermal management in solid polymer electrolyte fuel cells. *J Electrochem Soc.* 1993;140:1218.
4. Nguyen TV, White RE. A water and heat management model for proton exchange membrane fuel cells. *J Electrochem Soc.* 1993;140: 2178.
5. Springer TE, Rockward T, Zawodzinski TA, Gottesfeld S. Model for polymer electrolyte fuel cell operation on reformate feed: effects of CO, H2 dilution, high fuel utilization. *J Electrochem Soc.* 2001;148(1): A11.
6. Springer TE, Zawodzinski TA, Gottesfeld S. Polymer electrolyte fuel cell model. *J Electrochem Soc.* 1991;138:2334.
7. Um S, Wang CY. Three-dimensional analysis of transport and electrochemical reactions in polymer electrolyte fuel cells. *J Power Sources.* 2004;125:40.
8. Wang ZH, Wang CY. Mathematical modeling of liquid-feed direct methanol fuel cells. *J Electrochem Soc.* 2003;150:A508.
9. Bernardi DM, Verbrugge MW. A mathematical model of a gas diffusion electrode bonded to a polymer electrolyte. *AIChE J.* 1992;37: 2477.
10. Friedman DJ, Moore RM. Optimum operating curves for fuel cell systems. Record of the 1st Annual Fuel Cell Vehicle Technology Conference, University of California, Davis, CA, 1998.
11. Xu C, Follmann PM, Biegler LT, Jhon MS. Numerical simulation and optimization of a direct methanol fuel cell. *Computers Chem Eng.* 2005;29(8):1849-1860.
12. Godat J, Marechal F. Optimization of a fuel cell system using process integration techniques. *J Power Sources.* 2003;118:411.
13. Marechal F, Palazzi F, Godat J, Favrat D. Thermo-economic modeling and optimization of fuel cell systems. *Fuel Cells*. 2004;5, 1:5-24.
14. *Aspen Plus Documentation Version 11.1*. Cambridge, MA: Aspen Technology, Inc.; 2001.
15. Larminie J, Dicks A. *Fuel Cell Systems Explained*. New York: John Wiley; 2000.
16. Duran MA, Grossmann IE. Simultaneous optimization and heat integration of chemical processes. *AICHE J.* 1986;32:123.
17. Lang YD, Biegler LT, Grossmann IE. Simultaneous optimization and heat integration with process simulators. *Computers Chem Eng.* 1988; 12:311.
18. Yee TF, Grossmann IE, Kravanja Z. Simultaneous optimization models for heat integration. III. Optimization of process flowsheets and heat exchanger networks. *Computers Chem Eng.* 1990;14:1185.
19. Balakrishna S, Biegler LT. Targeting strategies for the synthesis and energy integration of nonisothermal reactor networks. *Ind Eng Chem Res.* 1992;31:2152.
20. Biegler LT, Grossmann IE, Westerberg AW. *Systematic Methods for Chemical Process Design*. Upper Saddle River, NJ: Prentice Hall; 1997.
21. Lutz AE, Bradshaw RW, Keller JO, Witmer DE. Thermodynamic analysis of hydrogen production by steam reforming. *Int J Hydrogen Energy.* 2003;28:159.
22. IES Group. *Process Utilities Cost Guide 2002*. Available at http://ed.icheme.org/costutil.html.

Manuscript received Mar. 13, 2005, and revision received Jan. 31, 2006.